AGU PUBLICATIONS

Global Biogeochemical Cycles

RESEARCH ARTICLE
10.1002/2016GB005400

Quantifying the drivers of ocean-atmosphere CO_2 fluxes

Jonathan M. Lauderdale[1], Stephanie Dutkiewicz[1,2], Richard G. Williams[3], and Michael J. Follows[1]

[1]Department of Earth, Atmospheric and Planetary Sciences, Massachusetts Institute of Technology, Cambridge, Massachusetts, USA, [2]Center for Global Change Science, Massachusetts Institute of Technology, Cambridge, Massachusetts, USA, [3]Department of Earth, Ocean and Ecological Sciences, School of Environmental Science, University of Liverpool, Liverpool, Merseyside, UK

Key Points:
- We have developed a quantitative framework for diagnosing regional drivers of air-sea CO_2 fluxes
- Components can be evaluated in a model or can be derived from operational data, climatologies, and ocean state estimates
- Model CO_2 fluxes result from a balance between air-sea heat fluxes, biological activity, and disequilibrium

Correspondence to:
J. M. Lauderdale,
jml1@mit.edu

Citation:
Lauderdale, J. M., S. Dutkiewicz, R. G. Williams, and M. J. Follows (2016), Quantifying the drivers of ocean-atmosphere CO_2 fluxes, *Global Biogeochem. Cycles*, *30*, doi:10.1002/2016GB005400.

Received 19 FEB 2016
Accepted 6 JUN 2016
Accepted article online 11 JUN 2016

Abstract A mechanistic framework for quantitatively mapping the regional drivers of air-sea CO_2 fluxes at a global scale is developed. The framework evaluates the interplay between (1) surface heat and freshwater fluxes that influence the potential saturated carbon concentration, which depends on changes in sea surface temperature, salinity and alkalinity, (2) a residual, disequilibrium flux influenced by upwelling and entrainment of remineralized carbon- and nutrient-rich waters from the ocean interior, as well as rapid subduction of surface waters, (3) carbon uptake and export by biological activity as both soft tissue and carbonate, and (4) the effect on surface carbon concentrations due to freshwater precipitation or evaporation. In a steady state simulation of a coarse-resolution ocean circulation and biogeochemistry model, the sum of the individually determined components is close to the known total flux of the simulation. The leading order balance, identified in different dynamical regimes, is between the CO_2 fluxes driven by surface heat fluxes and a combination of biologically driven carbon uptake and disequilibrium-driven carbon outgassing. The framework is still able to reconstruct simulated fluxes when evaluated using monthly averaged data and takes a form that can be applied consistently in models of different complexity and observations of the ocean. In this way, the framework may reveal differences in the balance of drivers acting across an ensemble of climate model simulations or be applied to an analysis and interpretation of the observed, real-world air-sea flux of CO_2.

1. Introduction

The atmospheric inventory of carbon is regulated on interannual and longer timescales by the ocean carbon reservoir, mediated by the exchanges of carbon dioxide across the air-sea interface. This exchange (1) is proportional to the difference in ocean and atmosphere partial pressures of CO_2, and its efficiency is a function of temperature, salinity, and wind speed, encapsulated in the gas transfer coefficient, K:

$$F_{CO_2} = K(pCO_2^{ocean} - pCO_2^{atm}) \quad (1)$$

In recent decades, coordinated observation campaigns and the compilation of local data sets have provided an unprecedented global view of the regional and seasonal changes in air-sea exchange of CO_2 (as illustrated in Figure 1a) based on measurements of atmospheric and surface ocean pCO_2, along with estimates of K [*Wanninkhof*, 1992; *Takahashi et al.*, 2002, 2009; *Wanninkhof et al.*, 2013]. This growing database provides a clear qualitative and quantitative view of the patterns and rates of the air-sea flux at regional and global scales.

Since atmospheric pCO_2 is globally mixed on timescales of a year or so, regional and seasonal variations reflect oceanic processes that drive surface pCO_2 levels away from equilibrium with the overlying atmosphere. These include changes in solubility due to surface heat fluxes and temperature variations, the biotic fixation of carbon, and the upwelling of carbon-rich deep waters [e.g., *Murnane et al.*, 1999; *Sarmiento et al.*, 2000; *Takahashi et al.*, 2002, 2009; *Ito and Follows*, 2013].

Though the total flux can be derived from information on the pCO_2 gradient, quantification of the relative contributions of each of these drivers of CO_2 flux is difficult at regional and global scales. At a few sites around the globe, notably the Hawaii Ocean Time-series (HOT) and the Bermuda Atlantic Time-series Station (BATS), comprehensive biogeochemical observations provide an explicit view of the contributions of physical and biological drivers to seasonal and annual air-sea carbon fluxes [*Bates*, 2001; *Gruber et al.*, 2002; *Bates et al.*, 2002; *Dore et al.*, 2003, 2009; *Quay and Stutsman*, 2003; *Keeling et al.*, 2004]. Models can be tested and constrained

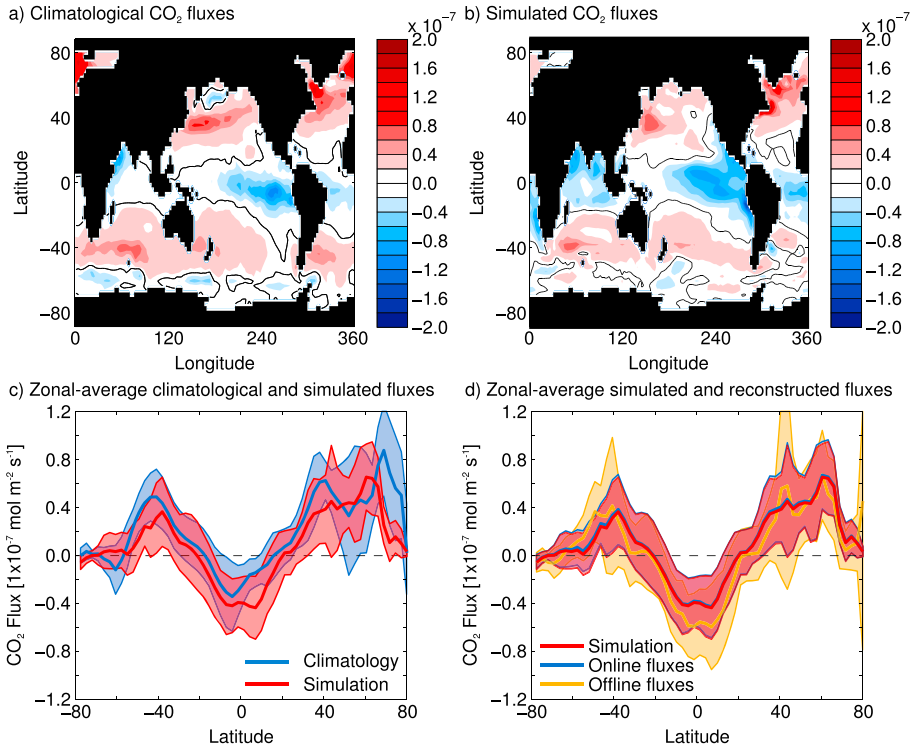

Figure 1. Air-sea CO_2 fluxes (mol C m^{-2} s^{-1}) for (a) the contemporary *Takahashi et al.* [2009] climatology (including anthropogenic carbon uptake) interpolated onto the same grid used by the model (approximately 3° × 3°), (b) simulated MITgcm preindustrial CO_2 fluxes using (1), (c) zonally averaged fluxes for the *Takahashi et al.* [2009] climatology (blue) and the model simulated preindustrial CO_2 fluxes (red) with ±1 standard deviation bounds to illustrate zonal variations, and (d) zonally averaged fluxes for the simulated Massachusetts Institute of Technology general circulation model (MITgcm) preindustrial CO_2 fluxes (red) and two reconstructions using the framework detailed in (8) with "online" advective and diffusive fluxes averaged into monthly fields (blue) and "off-line" advective and diffusive fluxes calculated with monthly average velocity, diffusivity, and scalar fields (orange). Again, ±1 standard deviation bounds are shown to illustrate zonal variations. Positive values indicate oceanic uptake, while negative values indicate outgassing.

by data from the time series sites and global surveys to reveal the contributions from biological and physical drivers [e.g., *Murnane et al.*, 1999; *Sarmiento et al.*, 2000; *Takahashi et al.*, 2002, 2009; *Schuster and Watson*, 2007; *Lovenduski et al.*, 2007; *Lovenduski and Ito*, 2009; *Corbiére et al.*, 2007; *Manizza et al.*, 2013].

A common starting point is to consider the rate of change of the concentration of dissolved inorganic carbon (C_T) in the surface ocean, which can be described as the balance of physical and biological processes:

$$\frac{\partial C_T}{\partial t} = -\nabla \cdot (\vec{u} C_T) + \nabla \cdot (\kappa \nabla C_T) - R_{C_T:P} S_{\text{bio}} - S_{\text{CaCO}_3} - \frac{F_w \overline{C_T}}{\rho_{\text{fw}} h} - \frac{F_{\text{CO}_2}}{h}, \tag{2}$$

Here the terms on the right-hand side describe the divergence of physical transport by advection and diffusion, including entrainment (terms one and two), biological sources and sinks of organic soft tissue and calcium carbonate (third and fourth terms), dilution by freshwater fluxes (fifth term), and, last but not least, the air-sea gas exchange of CO_2. Symbols are defined in detail in Table 1.

In cases where atmospheric CO_2 can be assumed constant, averaging over the seasonal cycle, $\partial C_T/\partial t$ approaches zero. Further integrating over the layer depth, h, we can rearrange (2) to explicitly relate the time-averaged air-sea exchange of CO_2 to the driving processes:

$$F_{\text{CO}_2} = -\nabla \cdot (\vec{u} C_T) h + \nabla \cdot (\kappa \nabla C_T) h - R_{C_T:P} S_{\text{bio}} h - S_{\text{CaCO}_3} h - \frac{F_w \overline{C_T}}{\rho_{\text{fw}}} \tag{3}$$

The individual terms can be evaluated in numerical models, where complete four-dimensional diagnostic information is available [e.g., *Lovenduski et al.*, 2013] (see also example in Appendix A). While such a breakdown provides an explicit quantification of each of the processes, its application is restricted to numerical

Table 1. Definition and Description of Terms in Equations

Term	Units	Description
F_{CO_2}	mol C m^{-2} s^{-1}	Air-sea flux of CO_2
K	mol C m^{-2} s^{-1} μatm^{-1}	Gas transfer coefficient
pCO_2^{ocean}	μatm	Surface ocean partial pressure of CO_2
pCO_2^{atm}	μatm	Atmospheric partial pressure of CO_2
C_T	mol C m^{-3}	Concentration of total dissolved inorganic carbon
t	s	Time
h	m	Layer depth
$\nabla\cdot$	m^{-1}	Divergence operator ($\partial/\partial x + \partial/\partial y + \partial/\partial z$)
$\vec{u}$	m s^{-1}	Three-dimensional ocean transport
κ	m^2 s^{-1}	Eddy diffusivity tensor
$R_{C_T:P}$	dimensionless	Biological transformation ratio between carbon and phosphate
P	mol P m^{-3}	Concentration of total dissolved inorganic phosphate
S_{bio}	mol P m^{-3} s^{-1}	Sources and sinks of biogenic soft tissue
S_{CaCO_3}	mol C m^{-3} s^{-1}	Sources and sinks of biogenic carbonate
F_w	kg m^{-2} s^{-1}	Net freshwater flux
$\overline{C_T}$	mol C m^{-3}	Mean surface carbon concentration
ρ_{fw}	kg m^{-3}	Density of freshwater
C_{sat}	mol C m^{-3}	Saturated concentration of carbon
$\gamma_\theta, \gamma_S, \gamma_{A_T}$	see Table 2	Carbon solubility coefficients for temperature, salinity, and alkalinity
C_{res}	mol C m^{-3}	Disequilibrium concentration carbon
θ	°C	Oceanic temperature
S	dimensionless	Salinity
A_T	mol eq m^{-3}	Alkalinity
F_{heat}	W m^{-2}	Air-sea heat flux
ρ	kg m^{-3}	Seawater density
C_p	J kg^{-1} $°C^{-1}$	Heat capacity of seawater
$\overline{S}$	dimensionless	Mean surface salinity
$\overline{A_T}$	mol eq m^{-3}	Mean surface alkalinity
R_{CaCO_3}	dimensionless	Organic to inorganic rain ratio in biogenic particles
$R_{N:P}$	dimensionless	Biological transformation ratio between nitrogen and phosphate
B	dimensionless	Revelle buffer factor

simulations since the required inputs are only sparsely covered by observations on the global scale. However, we can extend this approach to relate the driving terms in (3) to environmental fluxes and characteristics which are available in global climatologies and climate model diagnostics.

The purpose of this paper is to describe this extension and to test its validity and utility by diagnosing the drivers of CO_2 fluxes in a global numerical simulation.

Section 2 outlines the framework which links climatological physical forcing and ocean carbon reservoirs. In section 3 we test the framework by interpreting the contributions of different forcing processes in a numerical model simulation (described in section 2.2). We quantify the errors introduced in the interpretation when input data are limited to monthly averaged values, as we might encounter in applications to climatological observations or model comparison databases. Finally, in section 4, we discuss the prospects for wider application of the framework.

2. Methods: Diagnostic Framework and Testbed Simulation

Here we develop the extended diagnostic framework which quantitatively links physical and biological drivers to air-sea fluxes of CO_2. We also describe the global ocean carbon cycle simulation used to test the new diagnostic framework and its robustness to some underlying assumptions.

2.1. Relating Air-Sea CO_2 Flux to Surface Drivers and Ocean Carbon Reservoirs

Expressions relating carbon fluxes and drivers (3) can be combined with parameterizations linking the individual terms to fluxes and state variables that are available in observed climatologies and standard climate model products. We also leverage on biogeochemical diagnostic approaches typically used to understand the controls on deep ocean carbon reservoirs (or carbon "pumps," [*Brewer*, 1978; *Gruber et al.*, 1996; *Ito and Follows*, 2005; *Williams and Follows*, 2011]).

At the sea surface, the total dissolved inorganic carbon concentration, C^T, can be separated into the saturated component, C_{sat}, the concentration a water mass would have if at equilibrium with atmospheric pCO_2, and a residual concentration, C_{res}, reflecting the disequilibrium due to a variety of physical and biological processes [*Ito and Follows*, 2013]:

$$C_T = C_{\text{sat}} + C_{\text{res}} \,. \tag{4}$$

C_{sat} depends on atmospheric pCO_2 and sea surface temperature, salinity, and alkalinity. These relationships can be described assuming a linearization of carbonate chemistry [e.g., *Williams and Follows*, 2011]:

$$\delta C_{\text{sat}} \simeq \gamma_\theta \, \delta\theta + \gamma_S \, \delta S + \gamma_{A_T} \, \delta A_T + \delta \text{pCO}_2 \, \frac{\partial C_{\text{sat}}}{\partial \text{pCO}_2} \tag{5}$$

where γ_θ, γ_S, and γ_{A_T} are solubility constants which reflect the close to linear relationships between C_{sat} with temperature, salinity, and alkalinity. While the relationship with pCO_2 is highly nonlinear, for the purposes of this study we will be considering a fixed, uniform atmospheric pCO_2, so $\delta pCO_2 = 0$.

Substituting for C_{sat} from (4) and (5) into (3), we express the drivers of F_{CO2} in terms of changes in environmental characteristics.

$$\begin{aligned} F_{\text{CO}_2} = {} & \gamma_\theta \left(-\nabla\cdot(\vec{u}\theta) + \nabla\cdot(\kappa\nabla\theta)\right) \, h + \gamma_S \left(-\nabla\cdot(\vec{u}S) + \nabla\cdot(\kappa\nabla S)\right) \, h + \gamma_{A_T} \left(-\nabla\cdot(\vec{u}A_T) + \nabla\cdot(\kappa\nabla A_T)\right) \, h \\ & + \left(-\nabla\cdot(\vec{u}C_{\text{res}}) + \nabla\cdot(\kappa\nabla C_{\text{res}})\right) \, h - R_{C_T:P} S_{\text{bio}} h - S_{\text{CaCO}_3} h - \frac{F_w \overline{C_T}}{\rho_{\text{fw}}} \end{aligned} \tag{6}$$

The first three terms on the right couch convergences of physical and biogeochemical characteristics as drivers of CO_2 fluxes. We can, in turn, relate these convergences in terms of air-sea fluxes of heat and freshwater. Consider, for example, the governing equation for surface temperature:

$$\frac{\partial\theta}{\partial t} = -\nabla\cdot(\vec{u}\theta) + \nabla\cdot(\kappa\nabla\theta) - \frac{F_{\text{heat}}}{\rho C_p h} \tag{7}$$

Assuming steady state we can substitute $-\nabla\cdot(\vec{u}\theta) + \nabla\cdot(\kappa\nabla\theta) = (F_{\text{heat}}/\rho C_p h)$ into (6). Similar substitutions can be made, including reframing biological sources and sinks in terms of the divergence of the nutrient transport (see Appendix B for a detailed derivation):

$$\begin{aligned} F_{\text{CO}_2} = {} & \gamma_\theta \tfrac{F_{\text{heat}}}{\rho C_p} && \text{Heat flux} \\ & + \tfrac{F_W}{\rho_{\text{fw}}} \left(\gamma_S \overline{S} + \gamma_{A_T} \overline{A_T} - \overline{C_T}\right) && \text{Freshwater flux} \\ & - R_{C_T:P} \left(-\nabla\cdot(\vec{u}P) + \nabla\cdot(\kappa\nabla P)\right) \, h && \text{Organic matter sources and sinks} \\ & - \tfrac{1}{2} R_{\text{CaCO}_3} R_{C_T:P} \left(-\nabla\cdot(\vec{u}P) + \nabla\cdot(\kappa\nabla P)\right) \, h && \text{Calcium carbonate sources and sinks} \\ & + \left(-\nabla\cdot(\vec{u}C_{\text{res}}) + \nabla\cdot(\kappa\nabla C_{\text{res}})\right) \, h && \text{Transport of disequilibrium component} \end{aligned} \tag{8}$$

We have now expressed the air-sea flux as a set of components related to fluxes that are either evaluated operationally (such as surface heat fluxes) or which can be derived from climatologies and ocean state estimates (such as nutrient transports). Each term in (8) quantifies a specific process that drives a proportion of the air-sea flux of CO_2.

In (8), the first term on the right (first row) is the "potential" CO_2 flux due to heat fluxes [*Murnane et al.*, 1999; *Takahashi et al.*, 2002, 2009], which drive changes in C_{sat}, the solubility of CO_2. The second row of terms reflects the influence of surface evaporation and precipitation in three ways: the dilution of salinity and alkalinity,

both affecting C_{sat}, and the direct dilution of dissolved inorganic carbon, C_T. Notice that the dilution of C_T and alkalinity compensate: one acts to reduce pCO_2 solubility and the other to increase it. Both heat and freshwater fluxes, F_{heat} and F_W, are standard products of climate models and climatologies based on operational weather products [*Kistler et al.*, 2001; *Dee et al.*, 2011]. These drivers are quantified and reasonably well characterized.

The third row describes the production or remineralization of organic soft tissue with a carbon to phosphorus ratio $R_{C:P}$, integrated to depth h. Using the governing equation for phosphate (see Appendix B), we have linked biological sources and sinks to the divergence of the phosphate transport field. Advective and eddy-diffusive phosphate fluxes are easily obtained from ocean models and may be reconstructed offline (with some introduced error) if the flow field and phosphate concentration is known. Estimates may also be based on climatological distribution of phosphate (e.g., the World Ocean Atlas [*Garcia et al.*, 2014]) with flow field and mixing parameters based on ocean state estimates [*Wunsch and Heimbach*, 2007; *Forget*, 2010; *Forget et al.*, 2015]. We note that nitrate might equally well be the basis of the biological flux divergence estimate, depending on the currency of the model or data available. However, nitrogen fixation and denitrification make the interpretation of the flux divergences a little more uncertain.

The fourth row represents the production of calcium carbonate in the surface ocean linked simply to soft tissue production in the surface ocean by a simple constant rain ratio, R_{CaCO_3}, and integrated to depth h. This simple scaling holds in the upper ocean, although the full governing equation for alkalinity could be used (again, see Appendix B), to take into account the different dissolution profiles of organic and inorganic particles.

The fifth and final row describes the divergence of the transport of the disequilibrium carbon reservoir, C_{res}, defined here as $C_{res} = C_T - C_{sat}$. Below the surface mixed layer C_{res}, as defined, includes contributions from regenerated organic matter, whereas, when modeling the carbon reservoirs in the deep ocean, the regenerated pool is explicitly diagnosed [*Brewer*, 1978; *Gruber et al.*, 1996; *Williams and Follows*, 2011; *Lauderdale et al.*, 2013]. Thus, here the divergence of C_{res} transport includes three important effects: (i) the entrainment of subsurface waters rich in regenerated C_T that will drive outgassing (ii) changes in surface fluxes of heat and freshwater that affect CO_2 solubility. For example, while cooling implies a positive change in the saturated carbon and therefore ocean CO_2 uptake, in a limited time period this potential flux is not achieved so the CO_2 flux due to C_{res} is negative (outgassing) to compensate, and the time delay of air-sea carbon flux response which results in accumulation of significant disequilibrium and shifts the air-sea flux response downstream of the previous two influences.

C_{res} can be diagnosed in models or from climatological data (the GLODAP atlas [*Key et al.*, 2004]) by estimating C_{sat} and subtracting it from C_T. It is not currently possible to cleanly separate three factors that affect the C_{res} fluxes. This component will also accumulate small errors associated with linearization of the carbonate chemistry in (5).

Each of the terms has a clear, mechanistic interpretation, and we suggest that (8) is more informative than (3). Additionally, all of the terms are formulated so that they can be quantitatively mapped from climatological databases and standard output from appropriate carbon cycle models.

As a proof of concept, we interpret the relative role of physical and biological drivers on patterns of air-sea carbon flux in a coarse-resolution ocean circulation and biogeochemistry model simulation. This provides a test bed where the air-sea flux of CO_2 is calculated prognostically at every time step by the model, using equation (1). We test the sensitivity of the framework to the input data density: climatological ocean data which might be used as inputs typically resolves monthly variations. Using the numerical simulations, we ask whether a useful diagnosis could be made with inputs at such temporal resolution.

In the next subsection we briefly describe the numerical simulation which forms the test bed. The application is discussed in section 3.

2.2. Testbed Numerical Simulation

The test bed simulation is a coarse resolution (2.8°×2.8°, 15 vertical levels) version of the Massachusetts Institute of Technology general circulation model [MITgcm, *Marshall et al.*, 1997] with online biogeochemistry [*Dutkiewicz et al.*, 2006; *Parekh et al.*, 2006]. The configuration is similar to the control experiment in *Lauderdale et al.* [2013], using the *Gent and McWilliams* [1990] scheme with a constant thickness diffusivity of 1000 $m^2\ s^{-1}$ but with the addition of the nonlocal K-Profile Parameterization (KPP) mixing scheme [*Large et al.*, 1994] that

Table 2. Values of the Linear Solubility Coefficients Used in the Attribution of Saturated Carbon Changes[a]

Coefficient	Gradient	Units
γ_θ	−8.72	mmol C m^{-3} $°C^{-1}$
γ_S	−5.93	mmol C m^{-3} psu^{-1}
γ_{A_T}	0.81	mmol C $(mmol\ eq)^{-1}$

[a]Coefficients were empirically diagnosed by calculating C_{sat} over a range of values for temperature, salinity, or alkalinity while holding the others (including atmospheric CO_2) at surface mean values [*Lewis and Wallace*, 1998; *Goodwin and Lenton*, 2009; *Ito and Follows*, 2013] and finding the gradient by linear regression.

enhances diapycnal mixing in regions where the water column is convectively unstable (above the constant value of 5×10^{-5} m^2 s^{-1}), including entrainment due to mixed layer deepening.

Biological transformations between carbon and nutrients are related using the fixed stoichiometric ratios of $R_{C_T:N:P:O} = 117:16:1:-170$ [*Anderson and Sarmiento*, 1994] with a prescribed inorganic to organic rain ratio (R_{CaCO_3}) of 7% [*Yamanaka and Tajika*, 1997]. Air-sea fluxes of CO_2 are calculated prognostically using (1) and are dependent on the square of local wind speed [*Wanninkhof*, 1992]. The annually averaged atmospheric CO_2 is 281 μatm, and the total ocean-atmosphere carbon inventory is conserved as there is no riverine carbon input, sediment carbon burial, nor external CO_2 emissions (hence, we neglect the accumulation of anthropogenic CO_2 at this stage). The simulations examined here have been integrated for 25,000 years, coming to a clear thermodynamic and biogeochemical steady state.

Advective and diffusive fluxes of all state variables, surface fluxes of heat, and freshwater, as well as biological production and losses of dissolved and particulate organic carbon and calcium carbonate were evaluated at each time step and saved as monthly averaged fields (see Appendix A). This provides a complete set of inputs for application and verification of the diagnostic framework. Furthermore, we use monthly averaged physical and biogeochemical scalars, velocity, and diffusivity fields mimicking the data density of typically available climatologies, to calculate oceanic fluxes in "off-line" mode and then apply the diagnostic framework to discover if a useful diagnosis could be made with inputs at such a low temporal resolution.

3. Results and Discussion: Quantifying CO_2 Fluxes and Drivers

3.1. Simulated air-Sea Flux of CO_2

The global simulation qualitatively and quantitatively captures the magnitude and variation of the climatological, observed air-sea flux of CO_2 [*Takahashi et al.*, 2009, Figure 1a–c]. Some differences are expected since the climatology reflects the current, transient state of the carbon cycle (in the reference year 2000, atmospheric CO_2 was around 350 μatm), while the simulation is for the natural, preindustrial state (~280 μatm). In the climatology, uptake of anthropogenic carbon by the ocean is evident in the stronger, more widespread fluxes at high latitudes, relative to the simulation, as well as the slightly weaker outgassing at the equator. The simulation provides a plausible, self-consistent system for which all fluxes and state variables can be accurately quantified. In the following section, we infer the drivers of the simulated pattern using the framework outlined in (8).

3.2. Inferred CO_2 Flux and Drivers

We evaluated each of the terms in equation (8) in the numerical simulation using fluxes from each time step and averaged into monthly fields. Heat and freshwater fluxes were obtained from the model's physical boundary conditions. The saturated and disequilibrium components were evaluated following standard procedures [*Williams and Follows*, 2011] using C_T, θ, S, and A_T in the upper ocean, as well as the atmospheric pCO_2 of 281 μatm from the simulation. The solubility coefficients (γ_θ, γ_S, and γ_{A_T}) were determined (Table 2) by calculating C_{sat} over a range of values for temperature, salinity, or alkalinity while holding the others (including atmospheric CO_2) at model surface mean values [*Lewis and Wallace*, 1998; *Goodwin and Lenton*, 2009; *Ito and Follows*, 2013].

We integrated the terms in (8) over the upper 50 m, in order to map the individual driver distributions in terms of an air-sea carbon flux. The framework reveals that surface heat forcing (Figure 2a), the dilution of

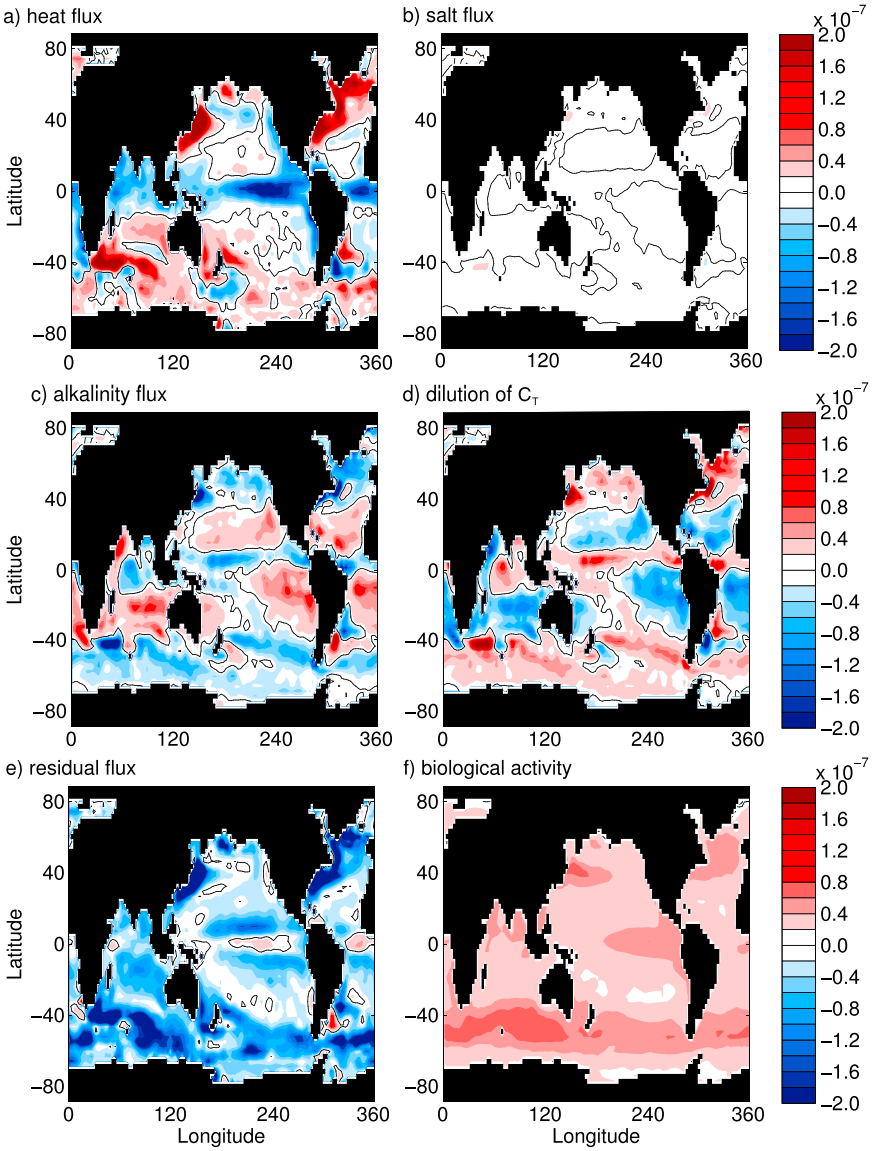

Figure 2. Component drivers of the air-sea flux of CO_2 (mol C m^{-2} s^{-1}) for the flux due to (a) surface heat fluxes $\left(\gamma_\theta \frac{F_{\text{heat}}}{\rho C_p}\right)$, (b) changes in salinity driven by freshwater fluxes $\left(\gamma_S \overline{S} \frac{F_W}{\rho_{\text{fw}}}\right)$, (c) changes in alkalinity driven by freshwater fluxes $\left(\gamma_{A_T} \overline{A_T} \frac{F_W}{\rho_{\text{fw}}}\right)$, (d) changes in carbon driven by freshwater fluxes $\left(\overline{C_T} \frac{F_W}{\rho_{\text{fw}}}\right)$, (e) divergence of total C_{res}, and (f) biological activity (soft tissue and carbonate terms, from divergence of nutrient concentration). Positive values indicate oceanic uptake from the atmosphere, while negative values indicate outgassing from the ocean.

alkalinity (Figure 2c) and C_T (Figure 2d), the divergent transport of C_{res} (Figure 2e), and biological sources and sinks (Figure 2f) are all of similar magnitude though with different patterns. The forcing due to dilution of salinity (Figure 2b) is much less significant. We also note that the dilution of alkalinity and C_T are strongly compensatory, as anticipated.

We can simplify the diagnostics, showing the leading order aggregated terms in Figure 3. The total reconstructed flux, F_{CO2} (Figure 3a), is largely accounted for by heat flux forcing of solubility (Figure 3b) and the sum of direct biological forcing and the divergence of C_{res} (Figure 3c). The compensation between C_{res} fluxes and biological forcing (Figures 2e and 2f) that lead us to group the drivers in this way is, in part, because biological carbon uptake is supported by the entrainment of regenerated nutrients, which simultaneously supplies regenerated carbon from the ocean interior to drive C_{res} outgassing [*Ito and Follows*, 2013].

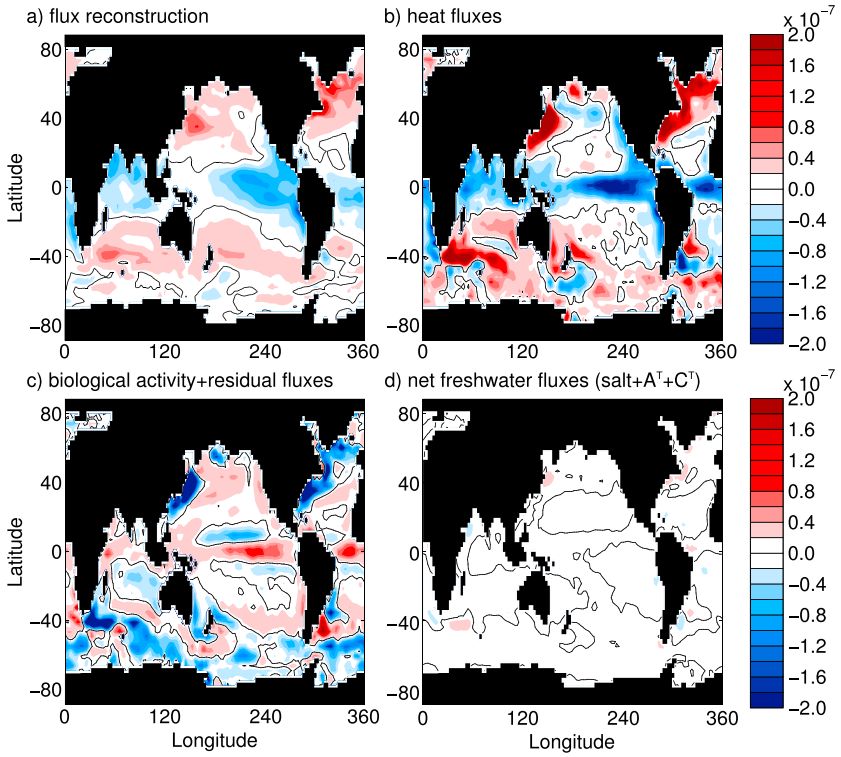

Figure 3. (a) reconstruction of the air-sea flux of CO_2 (mol C m^{-2} s^{-1}) as the sum of the component drivers, the majority of which is accounted for by (b) the CO_2 flux due to surface heat fluxes, and (c) the balance of the divergence of total C_{res} and the opposing flux due to biological activity. There is a negligible contribution from (d) the sum of CO_2 fluxes due to changes in salinity, alkalinity, and carbon concentrations that are all driven by net freshwater fluxes. Positive values indicate oceanic uptake from the atmosphere while negative values indicate outgassing from the ocean.

The biogenic-C_{res} compensation is far from complete on the local scale due to inefficiencies in biological activity, which may be restricted from full potential in some regions such as the Southern Ocean, limited by light and/or micronutrient concentrations [*Dutkiewicz et al.*, 2006]. Nevertheless, unutilized nutrients subducted from these regions may fuel a biological activity in other parts of the ocean through entrainment into the surface layer [*Sarmiento et al.*, 2004]. This is the case in most regions (Figure 2f), although, again, the C_{res} component is also affected by changes in solubility, particularly the cooling and rapid subduction of water masses from the surface. This would reinforce C_{res} outgassing at high latitudes because the potential saturated carbon uptake determined by the heat forcing is not achieved in the limited time at the surface, so that C_{res} is negative to compensate. Conversely, there are a few regions of C_{res}-driven uptake that correlate with patches of intense heat fluxes (warming, leading to outgassing in Figure 2a), which suggests that again, these surface waters are being rapidly advected downstream before local equilibration to the potential saturated concentration, determined by the heat forcing. There is a negligible contribution from the sum of CO_2 fluxes driven by the hydrological cycle, that is, changes in salinity and alkalinity, which affect C_{sat}, and changes in the C_T concentration (Figure 3d).

We note that the total flux evaluated as the sum of the individually quantified components accurately reflects F_{CO2} as calculated in the forward simulation (compare the maps in Figures 1b and 3a or the zonal average in Figure 1d). This is pleasing, indicating that no key processes have been overlooked (compared to the numerical simulation).

The global, annual average model-reconstruction difference is very small: -8×10^{-10} mol C m^{-2} s^{-1}, less than 1% of typical average fluxes locally and of the order of 0.1 PgC yr^{-1} integrated globally over 1 year (Table 3). Over this time frame, most of the components go to zero, which would be expected at steady state. Outgassing driven by C_{res} is closely compensated by the uptake driven by biological forcing, with a small residual probably representing a proportion of C_{res} linked to errors in linearization of the C_{sat} equation (5).

Table 3. Area-Integrated Carbon Flux Drivers (PgC yr^{-1})[a]

	Global	North Pacific and North Atlantic	Subtropical and Equatorial	Southern Ocean Midlatitudes	Southern Ocean South of 60°S
Heat Fluxes	0.00	1.02	−2.27	1.00	0.26
Salt Fluxes	−0.00	0.03	−0.08	0.02	0.03
Alkalinity Fluxes	−0.00	−0.24	0.73	−0.19	−0.29
Freshwater Fluxes	0.00	0.26	−0.77	0.21	0.31
Net Freshwater Fluxes	0.00	0.04	−0.13	0.03	0.05
Residual Flux	−6.63	−1.52	−1.84	−2.22	−1.06
Biological Activity	6.79	1.24	2.68	2.11	0.77
Residual + Biological	0.16	−0.29	0.84	−0.11	−0.29
Sum of Components	0.16	0.78	−1.56	0.92	0.02
Net CO_2 Flux	0.00	0.75	−1.60	0.87	−0.01

[a]The regions are divided by whether they are a net source or a net sink of CO_2 or neutral with respect to the zero contour of the simulated net air-sea CO_2 flux (see Figure 1b). Positive values indicate oceanic uptake of CO_2 from the atmosphere, while negative values indicate oceanic outgassing of CO_2 to the atmosphere.

When we use fluxes calculated offline using monthly averaged physical transports along with monthly averages of physical and biogeochemical concentrations to imitate climatological databases (Figure 1d), we find a degree of error is introduced, particularly leading to overestimation of equatorial outgassing and Southern Ocean uptake. Partly, there is an offset at midlatitudes (around 40°N/S) where the CO_2 flux framework slightly overestimates oceanic carbon uptake in the swift Gulf Stream, Kuroshio and Antarctic Circumpolar currents. This is not surprising since such regions will be prone to errors in the estimated flux divergence of C_{res} due to swift current and sharp gradients. Furthermore, uncertainty in vertical mixing of carbon and nutrients as a result of smoothing vertical concentration gradients leads to errors in the biological and disequilibrium terms. Nevertheless, the framework is still able to reconstruct the net air-sea CO_2 fluxes and their variation to a reasonable degree, which gives us confidence that careful application of (8) to climatological data and observations could warrant merit.

3.3. Regional Variations in the Drivers of Air-Sea CO_2 Fluxes

Having demonstrated that the diagnostic framework is able to capture the magnitude and regional variations in CO_2 fluxes, we now illustrate the application of the framework by quantifying the relative significance of different CO_2 flux drivers over several distinct regions of the simulated ocean. The results are summarized in Table 3.

We chose the aggregated regions according to whether they are a net source or sink or neutral with respect to atmospheric CO_2 (see the zero contour of the simulated net air-sea CO_2 flux in Figure 1b and the shaded regions in Figure 4). The regions are (i) the uptake region of the North Atlantic and North Pacific basins, the outgassing region of the tropics and subtropics, the region of uptake in the Southern Ocean midlatitudes (north of ~60°S to the zero CO_2 contour), and finally, the relatively neutral polar Southern Ocean, south of ~60°S.

A further decomposition also reveals some significant longitudinal patterns and is illustrated in Table 4 and Figure 4.

3.3.1. Northern Hemisphere (Oceanic Uptake)

In the North Pacific and North Atlantic the net CO_2 flux is into the ocean, as a result of solubility-driven uptake in the poleward flowing Gulf Stream and Kuroshio western boundary currents, which cool, and due to biological uptake. Disequilibrium-driven outgassing is large, which is a combination of strong convective mixing, particularly around southern Greenland, bringing remineralized carbon (and nutrients) to the surface, as well as subduction of surface waters into the ocean interior before coming to equilibrium with the atmosphere.

There are three different patterns governing zonal variation of CO_2 fluxes in the Northern Hemisphere (Figure 4a and Table 4):

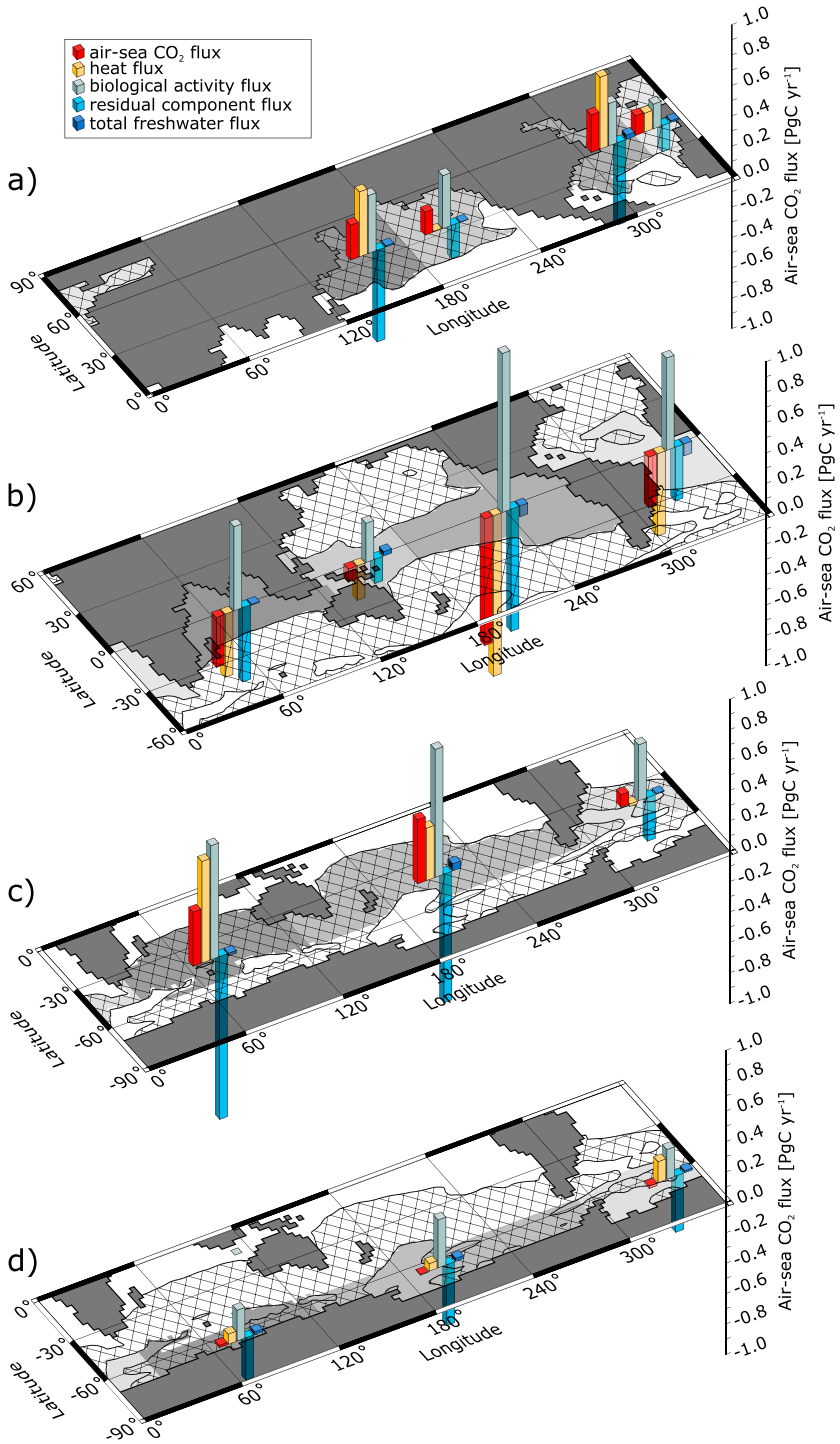

Figure 4. Area-integrated air-sea CO_2 fluxes (red) broken down into the CO_2 flux due to heat fluxes (yellow), biological activity (grey), the residual, C_{res}, component (light blue), and the total effect of freshwater fluxes (dark blue, the sum of salinity, alkalinity, and C_T changes) all in PgC yr^{-1}. Positive values indicate ocean uptake, while negative values indicate outgassing. The regions are primarily divided by whether they are a net source or a net sink of CO_2 as in Table 3, with ocean uptake of CO_2 occurring in the crosshatched regions, and further by the grey shaded areas of (a) the Northwest and Northeast regions of the Atlantic and Pacific, (b) the equatorial and subtropical Indian ocean, and the west and east regions of the Atlantic and Pacific, (c) the Indian, Pacific, and Atlantic midlatitude sectors of the Southern Ocean (north of ~60°S), and (d) the East Antarctic, Ross Sea, and Weddell Sea regions (south of ~60°S).

Table 4. Area-Integrated Carbon Flux Drivers (PgC yr^{-1})[a]

	CO_2 Flux	Heat Flux	Biological Activity	Residual Flux	Net FW Flux
Indian Ocean	−0.33	−0.42	0.56	−0.49	−0.01
Southern Ocean Indian Sector	0.36	0.67	0.75	−1.08	−0.02
East Antarctica	0.01	0.07	0.20	−0.28	0.02
NW Pacific	0.23	0.43	0.38	−0.61	0.01
NE Pacific	0.15	0.00	0.35	−0.22	0.00
West Equatorial Pacific	−0.09	−0.23	0.26	−0.16	0.03
East Equatorial Pacific	−0.84	−1.06	1.05	−0.81	-0.07
Southern Ocean Pacific Sector	0.42	0.35	0.85	−0.85	0.05
Ross Sea	0.00	0.05	0.32	−0.40	0.02
NW Atlantic	0.25	0.48	0.28	−0.55	0.03
NE Atlantic	0.13	0.12	0.16	−0.17	0.01
Equatorial Atlantic	−0.34	−0.55	0.61	−0.36	−0.08
Southern Ocean Atlantic Sector	0.08	−0.02	0.37	−0.29	0.00
Weddell Sea	−0.02	0.14	0.20	−0.37	0.01

[a]The regions are divided by whether they are a net source or a net sink of CO_2 or neutral with respect to the zero contour of the simulated net air-sea CO_2 flux and then by longitude (see shaded regions in Figure 4). Positive values indicate oceanic uptake of CO_2 from the atmosphere, while negative values indicate oceanic outgassing of CO_2 to the atmosphere.

1. In the western boundary current-dominated Northwest Pacific and Northwest Atlantic as mentioned above, the swift northward boundary current flow produces rapid cooling that is partially compensated by the subduction of mode waters that are incompletely equilibrated with the atmosphere causing negative C_{res} component fluxes. As a result, the absolute values of the disequilibrium fluxes are significantly larger than the opposing biologically driven fluxes.
2. In the Northeast Atlantic and high-latitude Northern Atlantic, the cooling of surface waters and deep water formation mostly drives the CO_2 uptake. This deep convective mixing, meanwhile, brings nutrient-rich waters to the surface that drives biological CO_2 uptake but also subducts deep waters from the surface before they have fully equilibrated with the atmosphere, again leading to outgassing disequilibrium fluxes.
3. In the more quiescent Northeast Pacific, CO_2 uptake is dominated by biological activity which is partially offset by the residual fluxes, with little influence of heat fluxes.

3.3.2. Equatorial-Subtropical Region (Oceanic Outgassing)

The equatorial-subtropical region generally outgases CO_2 to the atmosphere. Thermally driven outgassing is countered by net biologically driven CO_2 uptake, since individually, the residual component flux is completely counteracted by biological activity, although only partial equilibrium after heating may reduce the C_{res}-driven flux. Furthermore, assuming that all the nutrients required to drive the biological uptake are supplied by the equatorial upwelling, then suggests that these waters had outgased CO_2 when they were last in contact with the atmosphere. If this were not the case, the C_{res}-driven outgassing flux would closely balance the biologically driven uptake flux.

There are also longitudinal gradients in the regional drivers of the air-sea CO_2 flux at low latitudes, particularly in the west and east equatorial Pacific (Figure 4b and Table 4). The strongest upwelling of cool waters occurs in the east Pacific, associated with the sea surface temperature gradient and shoaling of the thermocline, with subsequently greater outgassing through warming due to heat fluxes. This is the region of strongest CO_2 outgassing, and its variability in the real ocean is heavily influenced by El Niño-La Niña conditions, associated with weakening (strengthening) of the longitudinal thermocline gradient and reduced (increased) upwelling of cool waters and residual carbon.

3.3.3. Southern Ocean Midlatitudes (Oceanic Uptake)

In southern midlatitudes, net uptake of CO_2 by the ocean occurs in all three basins (Table 3). Over the entire region, biologically driven CO_2 uptake is completely compensated by the C_{res}-driven outgassing, which are mechanistically linked, leaving CO_2 uptake driven by cooling to dominate the net flux.

Considering the zonal variation (Figure 4c and Table 4), the cooling flux is dominated by the Indian sector of the Southern Ocean where there is strong heat loss at the boundary between subtropical waters and the Antarctic Circumpolar Current, falling to one third of the size in the Pacific sector of the Southern Ocean. However, in the Indian Ocean sector the significant excess of C_{res}-driven outgassing compared to biologically driven uptake suggests that the cooling waters are incompletely equilibrated before subduction. Compare this to the Pacific sector, where biological activity closely compensates the residual flux.

The South Atlantic region as a whole displays a different pattern, with small heat flux-driven CO_2 fluxes (that actually suggest outgassing), leaving biological drivers to dominate the overall CO_2 uptake, incompletely compensated by C_{res}-driven outgassing. A patch of outgassing in the South Atlantic at 40°S (Figures 1b and 3a), which does not appear in the climatology (Figures 1a), may be a model artifact associated with the incorrect positioning of the subtropical front where the Antarctic Circumpolar Current (ACC) detaches from the coast of Argentina. Anomalously cold waters of the ACC would induce strong surface temperature relaxation in the model, which is seen in the heat flux-driven CO_2 flux component (Figure 3b). However, there is also a strong uptake flux associated with the C_{res} component (Figure 2e), suggesting that the swift current advects the surface waters into a neighboring cooling region before the warming effect is fully achieved. When integrated over the entire south Atlantic region, where cooling is also occurring in common with the rest of the Southern Ocean midlatitudes, the final result is that these opposing heat fluxes closely compensate in this region. Furthermore, the pattern of outgassing (due to upwelling of regenerated carbon) and uptake (due to incomplete equilibration to the saturated concentration determined by the heat forcing) in the disequilibrium component results in a comparatively small C_{res}-driven flux.

3.3.4. Southern Ocean South of 60°S (Neutral)

Finally, in the highest southern latitudes, south of roughly 60°S, the average flux is around zero (Table 3) although many of the individual components are significantly larger, indicating considerable compensation and interplay. Cooling of waters adjacent to Antarctica induces a positive CO_2 flux associated with the saturated carbon pool. The largest individual flux in this region comes from the residual, disequilibrium component driven by upwelling of deep waters rich in regenerated carbon and nutrients. While biological activity partly compensates, the net effect is negative (leading to outgassing) because the upwelled nutrients are incompletely utilized and biological activity is restricted from its full potential, limited by light and/or micronutrient concentrations. Additionally, cooling with incomplete equilibration may result in C_{res}-driven outgassing with the atmosphere before subduction into the deep ocean. In the Weddell Sea of this model in particular, there is a relatively strong CO_2 uptake associated with cooling due to heat fluxes, twice that of the East Antarctica and the Ross Sea regions, which is partly compensated by outgassing associated with the residual flux, suggesting the bottom waters formed here are incompletely equilibrated.

4. Summary and Outlook

We have developed diagnostic framework for interpreting the regional drivers of the air-sea flux of CO_2 which can be expressed succinctly and generally as

$$\begin{aligned} F_{CO_2} =& \gamma_\theta \frac{F_{\text{heat}}}{\rho C_p} + \frac{F_W}{\rho_{\text{fw}}}\left(\gamma_S \bar{S} + \gamma_{A_T}\overline{A_T} - \overline{C_T}\right) - R_{C_T:P}\left(-\nabla\cdot(\vec{u}P) + \nabla\cdot(\kappa\nabla P)\right)\ h \\ & - \frac{1}{2}R_{\text{CaCO}_3}R_{C_T:P}\left(-\nabla\cdot(\vec{u}P) + \nabla\cdot(\kappa\nabla P)\right)\ h + \left(-\nabla\cdot(\vec{u}C_{\text{res}}) + \nabla\cdot(\kappa\nabla C_{\text{res}})\right)\ h \end{aligned} \tag{9}$$

Drivers of the air-sea CO_2 flux are (1) The effect of heat and freshwater fluxes on the saturated ocean carbon concentration, which depends on surface temperature, salinity, and alkalinity at steady state atmospheric pCO_2; (2) the direct effect of freshwater dilution on surface C_T concentrations; and (3) carbon uptake and export by biological activity (as both soft tissue and carbonate) through nutrient utilization, and atmosphere-ocean disequilibrium, which is influenced by upwelling and entrainment of remineralized carbon- and nutrient-rich waters from the ocean interior as well as rapid subduction of surface waters before reaching full equilibrium.

Here in order to cleanly illustrate the framework, we have diagnosed the relative importance of air-sea flux drivers from a numerical model simulation. We demonstrated that the sum of the individually determined components is close to the known total flux of the simulation. In breaking down the contributions in the simulation, we find a dominant role for the air-sea heat flux forcing, as has been suggested by sensitivity experiments [*Follows et al.*, 1996; *Murnane et al.*, 1999; *Sarmiento et al.*, 2000; *Takahashi et al.*, 2002, 2009].

However, the analysis reveals that this is not universal, with a dominant role for biological- and air-sea disequilibrium-driven fluxes. In the upwelling regions of the Southern Ocean, the combined effect of biological activity and disequilibrium opposes the heat flux-driven CO_2 uptake. Here biological activity is limited from its maximum efficiency and so the upwelling of regenerated carbon is not completely compensated. Subduction of cooling waters before equilibrium also reinforces the C_{res} outgassing. In the equatorial upwelling regions, biological CO_2 uptake is generally larger than the disequilibrium-driven fluxes, offsetting the warming-driven outgassing.

Going beyond this proof-of-concept analysis of a single simulation, we believe that this diagnostic approach has potential for interesting applications. The approach could be applied offline with simulation data from climate models to reveal differences in the balance of drivers acting across an ensemble of simulations. Potentially more interesting still is the application to observed climatologies and the real-world air-sea flux of CO_2. Using monthly averaged fluxes calculated offline, the framework is still able to successfully reconstruct air-sea fluxes of CO_2 compared to the model simulation, albeit with a degree of error introduced into the biological activity and disequilibrium terms. Finally, there is also the prospect of extending the approach to include a time-varying atmospheric pCO_2. This is clearly challenging but should be explored.

In summary, we have developed and presented a new framework for analyzing the relative contributions of different physical and biogeochemical drivers to the air-sea flux of CO_2. Using numerical model simulations, where the correct solution is known, we have demonstrated that the method can work given appropriate input data. We suggest that applications to ensembles of model simulations and, in particular, climatological observations may be fruitful.

Appendix A: The Upper Ocean Carbon Budget

Taking the model surface layer of uniformly 50 m depth over which (2) is integrated, the carbon budget can be partitioned into six components, combining the effects of soft tissue and order of magnitude smaller carbonate biogenic activity (Figure A1). Divergence of the horizontal and vertical advective fluxes (including parameterized eddy bolus advection) taken separately is an order of magnitude larger than the sum (Figure A1a) and therefore show a large degree of compensation. For example, upwelling of carbon in the equatorial regions and the Southern Ocean is largely, but incompletely, redistributed by the horizontal gyre circulation leading to small, but significant, accumulation of carbon. Similarly, in the subtropical gyres there is convergence of C_T due to horizontal advection but this is counteracted by downwelling and deepened pycnoclines leading to net decrease in C_T.

Divergence of horizontal and vertical diffusive fluxes of C_T (Figure A1b) is almost entirely due to vertical diffusion, increasing C_T concentrations everywhere, but particularly elevated in the eastern equatorial Pacific, parts of the Southern Ocean and western boundary current regions where vertical gradients are large and convective mixing is important.

Upwelling of carbon to the surface is also accompanied by dissolved nutrients that drive widespread decrease in surface C_T concentrations due to biological fixation of carbon at the surface and vertical export to depth as sinking particles (Figure A1c). The rate of carbon concentration change here is prognostically calculated by the biogeochemical model as the net effect of biological productivity depending on the availability of light and nutrients, export fluxes, and remineralization of dissolved and particulate organic and inorganic matter. Biological activity particularly occurs in the equatorial and high-latitude oceans where nutrients are abundant in the model, although in some places limited by availability of light and micronutrients [e.g., *Dutkiewicz et al.*, 2006], with low biological drawdown in the oligotrophic subtropical gyres.

Net surface freshwater fluxes can induce changes in surface carbon concentration (Figure A1d). Regions where precipitation dominates (including relaxation to surface salinity climatology) such as low latitudes under the Intertropical convergence zone the C_T concentration is decreased through dilution, whereas in the subtropical regions where evaporation is the dominant process, C_T concentration increases by roughly the same amounts.

Accumulating the effects of advection, diffusion, biological activity, and freshwater fluxes leads to regions of net C_T accumulation or reduction at the surface, which drive oceanic pCO_2 variations and ultimately air-sea fluxes of CO_2. The CO_2 fluxes in Figure A1e (redrawn from Figure 1b) are computed by the biogeochemistry model using (1) and show outgassing in the equatorial-subtropical regions and uptake at the midlatitudes.

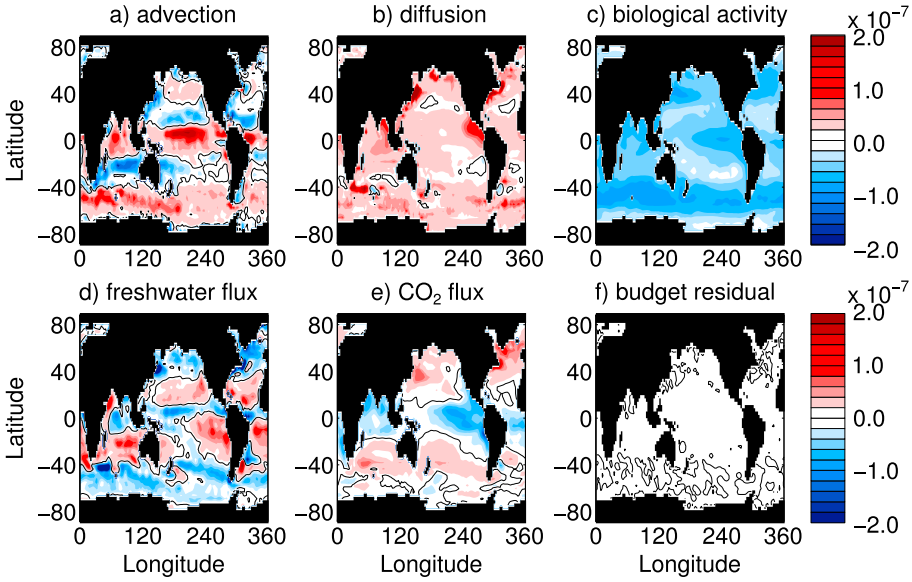

Figure A1. Upper ocean C_T budget: $0 = \nabla \cdot (\vec{u}C_T)h + \nabla \cdot (\kappa \nabla C_T)h + R_{C_T:P} S_{\text{bio}} h + \frac{1}{2} S_{\text{CaCO}_3} h + \frac{F_w \overline{C_T}}{\rho_{\text{fw}}} + F_{\text{CO}_2}$ (mol C m^{-2} s^{-1}) comprising (a) the divergence of three-dimensional advection of carbon, (b) divergence of horizontal and vertical diffusion of carbon, (c) biological activity (soft tissue and carbonate combined) directly calculated by the model, including biological community productivity, export fluxes, and remineralization of dissolved and particulate organic and inorganic matter, (d) the effect of freshwater fluxes (precipitation or evaporation) on the concentration or dilution of surface C_T concentrations, (e) the air-sea exchange of carbon dioxide using (1), and (f) the budget residual which is the sum of components in Figures A1a through A1e. Positive values indicate increasing carbon concentration tendency, while negative values indicate decreasing carbon concentration tendency. The location of the zero contour is plotted in black.

Appendix B: Development of the Carbon Flux Diagnostic Framework

This section lays out the specifics of the new, mechanistic carbon flux framework (8). Terms are defined and described in Table 1.

B1. Estimating the Effect of Biological Processes

Considering (3), the most difficult terms to infer are the effects of biological activity, S_{bio} and S_{CaCO_3}, on the surface flux of CO_2. A similar equilibrium relationship to (2) can be written considering the steady state phosphate concentration (B1), from which the S_{bio} component can be obtained from the advective and diffusive fluxes of nutrients (B2). Nitrate could also be used here instead.

$$\frac{\partial P}{\partial t} = -\nabla \cdot (\vec{u}P) + \nabla \cdot (\kappa \nabla P) - S_{\text{bio}} \tag{B1}$$

$$S_{\text{bio}} = -\nabla \cdot (\vec{u}P) + \nabla \cdot (\kappa \nabla P) \tag{B2}$$

Rearranging the steady state budget of alkalinity (A_T, B3) could yield a similar expression for the S_{CaCO_3} component from the advective and diffusive fluxes of alkalinity, the consumption of charged nutrients, and dilution or concentration of A_T by surface freshwater fluxes (B4).

$$\frac{\partial A_T}{\partial t} = -\nabla \cdot (\vec{u}A_T) + \nabla \cdot (\kappa \nabla A_T) - 2S_{\text{CaCO}_3} - R_{N:P} S_{\text{bio}} - \frac{F_w \overline{A_T}}{\rho_{\text{fw}} h} \tag{B3}$$

$$S_{\text{CaCO}_3} = \frac{1}{2}\left[-\nabla \cdot (\vec{u}A_T) + \nabla \cdot (\kappa \nabla A_T) - R_{N:P} S_{\text{bio}} - \frac{F_w \overline{A_T}}{\rho_{\text{fw}} h}\right] \tag{B4}$$

For simplicity, however, S_{CaCO_3} can also be estimated by assuming an organic carbon to inorganic carbonate production/remineralization ratio (R_{CaCO_3}), in which case

$$S_{\text{CaCO}_3} = \frac{1}{2} R_{\text{CaCO}_3} R_{C_T:P} S_{\text{bio}} \tag{B5}$$

B2. Saturated and Disequilibrium Carbon Reservoirs

The advective and diffusive fluxes of C_T in the carbon budget (3) can be further broken down into several different constituents, linking surface carbon fluxes to interior carbon reservoirs [*Brewer*, 1978; *Gruber et al.*, 1996; *Ito and Follows*, 2005; *Williams and Follows*, 2011]. In turn, this allows atmosphere-ocean carbon fluxes to be linked to physical forcing of the ocean.

At the sea surface, a parcel of water in chemical equilibrium with the atmosphere will have a dissolved carbon concentration equal to the saturated concentration, C_{sat} (B6). However, since CO_2 gas exchange is not instantaneous, having a timescale of the order of 1 year [*Ito et al.*, 2004], there will be a residual disequilibrium concentration, C_{res}, which results from other processes that drive the surface C_T concentration away from the "potential" chemical equilibrium concentration. This measure of incomplete air-sea gas exchange is largely influenced by the upwelling of regenerated carbon of biogenic origin from the deep ocean [*Ito and Follows*, 2013] and rapid subduction of waters from the surface before equilibration with the atmosphere. In some regions, outside the surface layer, there may also be a contribution to C_T from the remineralization of sinking soft tissue (C_{soft}) and carbonate (C_{carb}) particles of biogenic origin, however these reservoirs are zero by definition in the surface ocean.

$$C_T = C_{sat} + C_{res} \tag{B6}$$

The concentration of C_{sat} in the surface ocean depends on atmospheric pCO_2 and the surface temperature, salinity and alkalinity. Again, away from the surface ocean there is a contribution to the alkalinity from remineralization of calcium carbonate particles and addition of charged nutrients ($A_T = A_{pre} + A_{reg}$); however, these reservoirs are zero by definition in the surface ocean.

It is possible to separate the individual effects of the latter three terms by linearizing the buffering capacity of seawater at constant pCO_2 such that perturbations of C_{sat} can be evaluated from surface changes in θ, S, and A_T (B7).

$$\delta C_{sat} \simeq \gamma_\theta\, \delta\theta + \gamma_S\, \delta S + \gamma_{A_T}\, \delta A_T + \delta pCO_2 \frac{\overline{C_{sat}}}{B pCO_2} \tag{B7}$$

The solubility coefficients (γ_θ, γ_S, and γ_{A_T}) that represent the tight linear relationships between equilibrium carbon concentrations and forcing can be determined by calculating C_{sat} over a range of values for temperature, salinity, or alkalinity while holding the others (including atmospheric CO_2) at surface mean values [*Lewis and Wallace*, 1998; *Goodwin and Lenton*, 2009; *Ito and Follows*, 2013] (Table 2).

The relationship between C_{sat} and pCO_2 is nonlinear due to the buffering capacity of seawater, and an expression involving the Revelle buffer factor, B, is required [*Ito and Follows*, 2005; *Goodwin et al.*, 2007] to correctly diagnose changes in the saturated carbon associated with changes in atmospheric CO_2 (B8); however, we do not develop this part of the framework, keeping atmospheric CO_2 at a constant value in (5) neglecting anthropogenic carbon emissions.

$$B = \left(\frac{\delta pCO_2}{\delta \overline{C_T}}\right)\left(\frac{\overline{C_T}}{pCO_2}\right) \tag{B8}$$

Thus, the concentration of C_{sat} can be diagnosed for other data sources as will be described in the next section; however, knowledge of C_T is still needed to determine C_{res} using (B6).

B3. Evaluating Individual Components of the Saturated Carbon Flux

Individual contributions from $\delta\theta$, δS, and δA_T (B7) to the potential equilibrium air-sea CO_2 flux can be calculated from the steady state budgets for temperature (B9), salinity (B10), and alkalinity (B11). Note that the biological formation of calcium carbonate is not included in the alkalinity equation because the dominant balance at steady state is between the fluxes of alkalinity due to ocean circulation and air-sea freshwater fluxes. Biological fluxes are an order-of-magnitude smaller. The dominance of freshwater at the surface produces a close linear relationship between surface concentrations of alkalinity and salinity. This does not suggest that we totally disregard the small contribution of calcium carbonate cycling in the surface layer, but by the definition of (B6), we have instead partitioned it into the C_{res} pool. This is consistent with the treatment of the biological fixation of soft tissue carbon, which is also accounted for in the disequilibrium pool since increased productivity drives undersaturation of C_T, making the concentration of C_{res} more negative, which leads to CO_2 uptake.

$$\frac{\partial\theta}{\partial t} = -\nabla\cdot(\vec{u}\theta) + \nabla\cdot(\kappa\nabla\theta) - \frac{F_{heat}}{\rho C_p h} \tag{B9}$$

$$\frac{\partial S}{\partial t} = -\nabla \cdot (\vec{u}S) + \nabla \cdot (\kappa \nabla S) - \frac{F_w \bar{S}}{\rho_{\mathrm{fw}} h} \tag{B10}$$

$$\frac{\partial A_T}{\partial t} = -\nabla \cdot (\vec{u}A_T) + \nabla \cdot (\kappa \nabla A_T) - \frac{F_w \overline{A_T}}{\rho_{\mathrm{fw}} h} \tag{B11}$$

At steady state, setting $\partial\theta/\partial t$, $\partial S/\partial t$, and $\partial A_T/\partial t$ to zero, the changes in saturated carbon ($\delta\theta$, δS, and δA_T) and the residual carbon concentrations can be inferred directly from surface heat and freshwater fluxes and substituted in (2) and (3) for the advective and diffusive fluxes of C_T (B12).

$$\nabla \cdot (\kappa \nabla C_T) - \nabla \cdot (\vec{u}C_T) = \frac{\gamma_\theta F_{\mathrm{heat}}}{\rho C_p} \frac{F_W}{\rho_{\mathrm{fw}}} \left(\gamma_S \bar{S} + \gamma_{A_T} \overline{A_T} \right) - \nabla \cdot (\vec{u}C_{\mathrm{res}}) + \nabla \cdot (\kappa \nabla C_{\mathrm{res}}) \tag{B12}$$

Again, note that the contributions to the saturated carbon exchange due to temperature, salinity, and alkalinity are potential fluxes that are only fully realized at chemical equilibrium. In reality, the individual temperature, salinity, and alkalinity fluxes will only be partially fulfilled, with the remainder collected in the residual, disequilibrium flux (C_{res}).

Drawing together these different components into (3) with the additional parameters from (B2), (B5), (B6), and (B12) substituted for the soft tissue and carbonate components of biological activity, saturated carbon advection, diffusion from temperature, salinity, and alkalinity surface forcing, and finally C_{res}, which results from other processes such as upwelling into the surface layer that drive the surface C_T concentration away from equilibrium, gives a new quantitative, mechanistic framework to diagnose regional drivers of the global air-sea CO_2 fluxes (8).

Acknowledgments
J.M.L., S.D., and M.J.F. are grateful for funding from U.S. NSF grant OCE-1259388, while R.G.W. was supported by UK NERC grant NE/K012789/1. We thank Tim DeVries and an anonymous reviewer for their comments on our manuscript. Numerical model results and diagnostic routines are available from the author by request (jml1@mit.edu).

References

Anderson, L. A., and J. L. Sarmiento (1994), Redfield ratios of remineralization determined by nutrient data analysis, *Global Biogeochem. Cycles*, *8*, 65–80.

Bates, N. R. (2001), Interannual variability of oceanic CO_2 and biogeochemical properties in the western North Atlantic subtropical gyre, *Deep Sea Res., Part II*, *48*, 1507–1528, doi:10.1016/S0967-0645(00)00151-X.

Bates, N. R., A. C. Pequignet, R. J. Johnson, and N. Gruber (2002), A short-term sink for atmospheric CO_2 in subtropical mode water of the North Atlantic ocean, *Nature*, *420*, 489–493.

Brewer, P. (1978), Direct observation of oceanic CO_2 increase, *Geophys. Res. Lett.*, *5*, 997–1000.

Corbiére, A., N. Metzl, G. Reverdin, C. Brunet, and T. Takahashi (2007), Interannual and decadal variability of the oceanic carbon sink in the North Atlantic subpolar gyre, *Tellus B*, *59*, 168–178, doi:10.1111/j.1600-0889.2006.00232.x.

Dee, D. P., et al. (2011), The ERA-interim reanalysis: Configuration and performance of the data assimilation system, *Q. J. R. Meteorol. Soc.*, *137*, 553–597, doi:10.1002/qj.828.

Dore, J. E., R. Lukas, D. W. Sadler, and D. M. Karl (2003), Climate-driven changes to the atmospheric CO_2 sink in the subtropical North Pacific ocean, *Nature*, *424*, 754–757.

Dore, J. E., R. Lukas, D. W. Sadler, M. J. Church, and D. M. Karl (2009), Physical and biogeochemical modulation of ocean acidification in the central North Pacific, *Proc. Natl. Acad. Sci. U.S.A.*, *106*, 12,235–12,240.

Dutkiewicz, S., M. J. Follows, P. Heimbach, and J. Marshall (2006), Controls on ocean productivity and air–sea carbon flux: An adjoint model sensitivity study, *Geophys. Res. Lett.*, *33*, L02603, doi:10.1029/2005GL024987.

Follows, M. J., R. G. Williams, and J. C. Marshall (1996), The solubility pump of carbon in the subtropical gyre of the North Atlantic, *J. Mar. Res.*, *54*, 605–630.

Forget, G. (2010), Mapping ocean observations in a dynamical framework: A 2004–06 Ocean Atlas, *J. Phys. Oceanogr.*, *40*, 1201–1221, doi:10.1175/2009JPO4043.1.

Forget, G., J. M. Campin, P. Heimbach, C. N. Hill, R. M. Ponte, and C. Wunsch (2015), ECCO version 4: An integrated framework for non-linear inverse modeling and global ocean state estimation, *Geosci. Model Dev.*, *8*, 3071–3104, doi:10.5194/gmd-8-3071-2015.

Garcia, H. E., R. A. Locarnini, T. P. Boyer, J. I. Antonov, O. Baranova, M. Zweng, J. Reagan, and D. Johnson (2014), World Ocean Atlas 2013, in *Volume 4: Dissolved Inorganic Nutrients (Phosphate, Nitrate, Silicate), NOAA Atlas NESDIS 76*, edited by S. Levitus and A. Mishonov, pp. 1–25, U.S. Dep. of Commer. Silver Spring, Md.

Gent, P. R., and J. McWilliams (1990), Isopycnal mixing in ocean circulation models, *J. Phys. Oceanogr.*, *20*, 150–155.

Goodwin, P., and T. M. Lenton (2009), Quantifying the feedback between ocean heating and CO_2 solubility as an equivalent carbon emission solubility as an equivalent carbon emission, *Geophys. Res. Lett.*, *36*, L15609, doi:10.1029/2009GL039247.

Goodwin, P., R. G. Williams, M. J. Follows, and S. Dutkiewicz (2007), Ocean-atmosphere partitioning of anthropogenic carbon dioxide on centennial timescales, *Global Biogeochem. Cycles*, *21*, GB1014, doi:10.1029/2006GB002810.

Gruber, N., J. L. Sarmiento, and T. F. Stocker (1996), An improved method for detecting anthropogenic CO_2 in the oceans, *Global Biogeochem. Cycles*, *10*, 809–837.

Gruber, N., C. D. Keeling, and N. R. Bates (2002), Interannual variability in the North Atlantic Ocean carbon sink, *Science*, *298*, 2374–2378.

Ito, T., and M. J. Follows (2005), Preformed phosphate, soft tissue pump and atmospheric CO_2, *J. Mar. Res.*, *63*, 813–839.

Ito, T., and M. J. Follows (2013), Air-sea disequilibrium of carbon dioxide enhances the biological carbon sequestration in the Southern Ocean, *Global Biogeochem. Cycles*, *27*, 1129–1138, doi:10.1002/2013GB004682.

Ito, T., J. Marshall, and M. J. Follows (2004), What controls the uptake of transient tracers in the Southern Ocean?, *Global Biogeochem. Cycles*, *18*, GB2021, doi:10.1029/2003GB002103.

Keeling, C. D., H. Brix, and N. Gruber (2004), Seasonal and long-term dynamics of the upper ocean carbon cycle at station ALOHA near Hawaii, *Global Biogeochem. Cycles*, *18*, GB4006, doi:10.1029/2004GB002227.

Key, R. M., A. Kozyr, C. L. Sabine, K. Lee, R. Wanninkhof, J. L. Bullister, R. A. Feely, F. J. Millero, C. Mordy, and T. H. Peng (2004), A global ocean carbon climatology: Results from the global data analysis project GLODAP, *Global Biogeochem. Cycles*, *18*, GB4031, doi:10.1029/2004GB002247.

Kistler, R., et al. (2001), The NCEP–NCAR 50-year reanalysis: Monthly means CD–ROM and documentation, *Bull. Am. Meteorol. Soc.*, *82*, 247–267, doi:10.1175/1520-0477.

Large, W. G., J. C. McWilliams, and S. C. Doney (1994), Oceanic vertical mixing: A review and a model with a nonlocal boundary layer parameterization, *Reviews of Geophysics*, *32*, 363–403, doi:10.1029/94RG01872.

Lauderdale, J. M., A. C. Naveira Garabato, K. I. C. Oliver, M. J. Follows, and R. G. Williams (2013), Wind-driven changes in Southern Ocean residual circulation, ocean carbon reservoirs and atmospheric CO_2, *Clim. Dyn.*, *41*, 2145–2164, doi:10.1007/s00382-012-1650-3.

Lewis, E., and D. W. R. Wallace (1998), A program developed for CO_2 system calculations, Tech. Rep. ORNL/CDIAC-105, Carbon Dioxide Inf. Anal. Center, Oak Ridge Natl. Lab., Oak Ridge, Tennessee.

Lovenduski, N. S., and T. Ito (2009), The future evolution of the Southern Ocean CO_2 sink, *J. Mar. Res.*, *67*, 597–617, doi:10.1357/002224009791218832.

Lovenduski, N. S., N. Gruber, S. C. Doney, and I. D. Lima (2007), Enhanced CO_2 outgassing in the Southern Ocean from a positive phase of the Southern Annular Mode, *Global Biogeochem. Cycles*, *21*, GB2026, doi:10.1029/2006GB002900.

Lovenduski, N. S., M. C. Long, P. R. Gent, and K. Lindsay (2013), Multi-decadal trends in the advection and mixing of natural carbon in the Southern Ocean, *Geophys. Res. Lett.*, *40*, 139–142, doi:10.1029/2012GL054483.

Manizza, M., M. J. Follows, S. Dutkiewicz, D. Menemenlis, C. N. Hill, and R. M. Key (2013), Changes in the Arctic Ocean CO_2 sink (1996–2007): A regional model analysis, *Global Biogeochem. Cycles*, *27*, 1108–1118, doi:10.1002/2012GB004491.

Marshall, J., A. Adcroft, C. Hill, L. Perelman, and C. Heisey (1997), A finite-volume, incompressible Navier Stokes model for studies of the ocean on parallel computers, *J. Geophys. Res.*, *102*, 5753–5766.

Murnane, R. J., J. L. Sarmiento, and C. Le Quéré (1999), Spatial distribution of air-sea CO_2 fluxes and the interhemispheric transport of carbon by the oceans, *Global Biogeochem. Cycles*, *13*, 287–305, doi:10.1029/1998GB900009.

Parekh, P., M. J. Follows, S. Dutkiewicz, and T. Ito (2006), Physical and biological regulation of the soft tissue carbon pump, *Paleoceanography*, *21*, PA3001, doi:10.1026/2005PA001258.

Quay, P., and J. Stutsman (2003), Surface layer carbon budget for the subtropical North Pacific: $\delta^{13}C$ constraints at station ALOHA, *Deep Sea Res., Part I*, *50*, 1045–1061, doi:10.1016/S0967-0637(03)00116-X.

Sarmiento, J. L., P. Monfray, E. Maier-Reimer, O. Aumont, R. J. Murnane, and J. C. Orr (2000), Sea-air CO_2 fluxes and carbon transport: A comparison of three ocean general circulation models, *Global Biogeochem. Cycles*, *14*, 1267–1281, doi:10.1029/1999GB900062.

Sarmiento, J. L., N. Gruber, M. A. Brzezinski, and J. P. Dunne (2004), High latitude controls of thermocline nutrients and low latitude biological productivity, *Nature*, *427*, 56–60.

Schuster, U., and A. J. Watson (2007), *A Variable and Decreasing Sink for Atmospheric CO_2 in the North Atlantic*, vol. 112, C11006.

Takahashi, T., et al. (2002), Global sea-air CO_2 flux based on climatological surface ocean pCO_2 and seasonal biological and temperature effects, *Deep Sea Res., Part II*, *49*, 1601–1622.

Takahashi, T., et al. (2009), Climatological mean and decadal change in surface ocean pCO_2, and net sea–air CO_2 flux over the global oceans, *Deep Sea Res., Part II*, *56*, 554–577, doi:10.1016/j.dsr2.2008.12.009.

Wanninkhof, R. (1992), Relationship between wind speed and gas exchange over the ocean, *J. Geophys. Res.*, *97*, 7373–7382.

Wanninkhof, R., et al. (2013), Global ocean carbon uptake: Magnitude, variability and trends, *Biogeosciences*, *10*, 1983–2000, doi:10.5194/bg-10-1983-2013.

Williams, R. G. G., and M. J. Follows (2011), *Ocean Dynamics and the Carbon Cycle: Principals and Mechanisms*, Cambridge Univ. Press, Cambridge, U. K.

Wunsch, C., and P. Heimbach (2007), Practical global oceanic state estimation, *Physica D*, *230*, 197–208, doi:10.1016/j.physd.2006.09.040.

Yamanaka, Y., and E. Tajika (1997), Role of dissolved organic matter in the marine biogeochemical cycle: Studies using an ocean biogeochemical general circulation model, *Global Biogeochem. Cycles*, *11*, 599–612.